ACS OMEGA

Open Access

http://pubs.acs.org/journal/acsodf

Article

Structural and Electric Characterization of Sputtered Pt/WSe_2 Contacts toward High-Performance 2D p-FETs

Ryuichi Nakajima, Tomonori Nishimura, Kaito Kanahashi, Shogo Hatayama, Wen Hsin Chang, Yuta Saito, Toshifumi Irisawa, Keiji Ueno, Yasumitsu Miyata, Takashi Taniguchi, Kenji Watanabe, and Kosuke Nagashio*

Cite This: *ACS Omega* 2025, 10, 42973−42979

Read Online

ACCESS | Metrics & More | Article Recommendations | Supporting Information

ABSTRACT: For high-performance p-type field-effect transistors (FETs) based on two-dimensional (2D) materials, the use of Pt as the contact metal, with its high work function, is advantageous for effective hole injection into the 2D channel. However, the high-energy sputtering process required to deposit Pt, due to its high melting point, often induces significant damage to the 2D materials. Recently, the achievement of nearly ideal van der Waals contacts in Sb_2Te_3/MoS_2 via sputtering has motivated us to investigate WSe_2 p-FETs with sputtered Pt electrodes. Notably, reasonable p-FET performance was observed even in monolayer WSe_2. However, various characterizations revealed that the crystal structure of WSe_2 was no longer preserved, suggesting the formation of a quasi-edge contact between Pt-sputtered WSe_2 and the WSe_2 channel. Moreover, from the perspective of sputtering applicability, the relationship between deposition methods, deposited materials, and the resulting extent of damage was systematically examined.

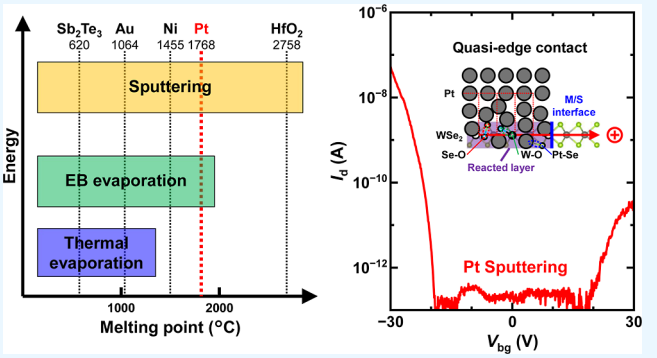

INTRODUCTION

Two dimensional (2D) layered materials, particularly transition metal dichalcogenides (TMDCs) such as MoS_2, WS_2, and WSe_2, hold significant potential for next-generation field-effect transistors (FETs)[1] because the atomic thickness of their channels is tolerant against short channel effects and the high on-state current can be retained even in the monolayer (1L) limit.[2] To realize complementary metal oxide semiconductor (CMOS) circuits composed entirely of 2D FETs, both high-performance 2D n-type and p-type FETs are necessary. While high-performance 2D n-FETs have been achieved,[3,4] such superior characteristics of 2D p-FETs remain limited.[5] It should be noted that the operation mechanism of 2D FETs is based on a Schottky barrier (SB) transistor, whose operation mode and performance are primarily influenced by the current injection through the SB at the metal/2D channel interface,[6,7] as opposed to a metal oxide semiconductor FET (MOSFET). This introduces a key challenge for high-performance 2D p-FETs: reducing the Schottky barrier height (SBH) between the Fermi level of metal electrodes with a high work function (WF) and the valence band of the 2D channel for efficient hole injection. A well-known issue in this regard is Fermi level pinning (FLP) at the metal/2D channel interface, where the Fermi level of metal electrodes is forcefully pinned close to the conduction band edge of 2D materials regardless of metal WFs, especially in MoS_2 cases.[8−10] However, prior studies on WSe_2 FETs indicate that their operation mode could be controlled by metal WF without significant treatment of the metal deposition method, suggesting that the strength of FLP in WSe_2 is relatively mild compared to the case of MoS_2.[11] Since the FLP is generally attributed to both the intrinsic mechanism and extrinsic defects in semiconductors, it is essential to explore deposition methods for metal electrodes with high WF.

Platinum (Pt) with the highest work function (∼5.7 eV) among stable single-element metals[12] is considered as a promising candidate for FET electrodes to demonstrate high-performance p-FETs. However, due to its high melting point (∼1768 °C) and low vapor pressure, only electron beam (EB) evaporation or sputtering can be employed for physical deposition, as illustrated in Figure 1a. These deposition methods typically lead to significant defect formation on 2D materials,[13−17] potentially causing severe FLP at the metal/2D channel interface or degradation of the transport properties of the 2D channels. Consequently, when Pt was utilized as electrodes for 2D channels, relatively thick multilayer

Received: June 17, 2025
Revised: August 26, 2025
Accepted: September 5, 2025
Published: September 15, 2025

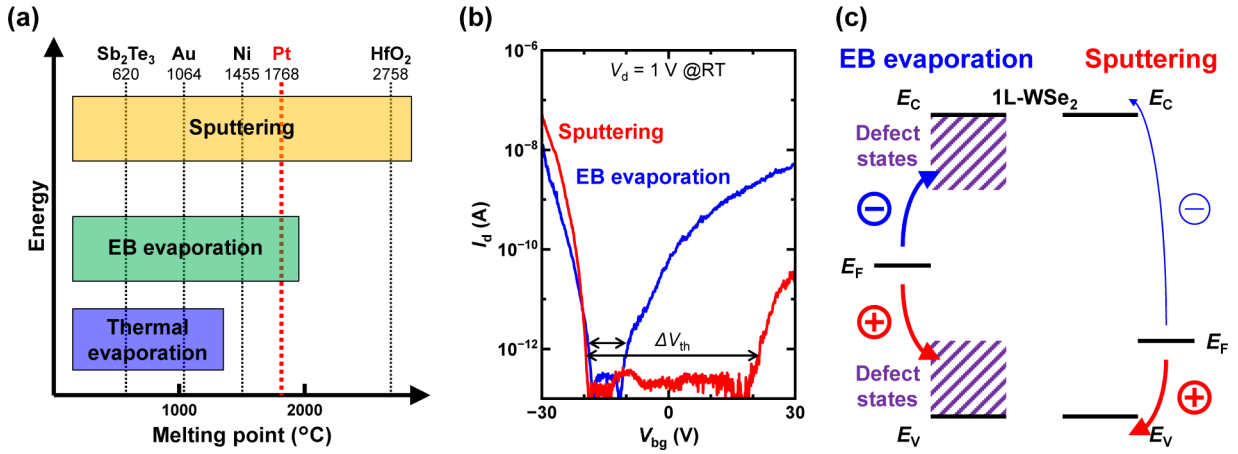

Figure 1. (a) Schematic illustration of the relationship between the melting points of the deposited materials and the various deposition techniques. (b) I_d−V_{bg} characteristic of 1L-WSe_2 FETs with Pt electrodes deposited by EB evaporation or sputtering, measured at a constant drain bias voltage (V_d) of 1 V at RT. (c) Schematic representation of the band alignment at the Pt/WSe_2 interfaces, derived from I_d−V_{bg} curves, for both EB evaporation and sputtering techniques.

films,[8,18−24] transferred electrodes,[10,25] and preprepared bottom electrodes[26,27] were employed to mitigate these issues. Nevertheless, p-FET operation in 1L-WSe_2 has been demonstrated with Pt electrodes deposited via rapid EB evaporation with long pauses to maintain the substrate temperature at room temperature (RT).[28] Furthermore, nearly ideal van der Waals (vdW) contacts have been reported for Sb_2Te_3/MoS_2 and Bi_2Te_3/WSe_2 by applying a conventional sputtering method.[29,30] In this research, therefore, we investigated the FET performance of 1L and bilayer (2L) WSe_2 FETs with sputtered Pt electrodes and the impact of Pt sputtering-induced damage on WSe_2.

RESULTS AND DISCUSSION

First, the impact of deposition methods on FET performance is compared. 1L-WSe_2 was prepared on a 90 nm SiO_2/n^+-Si substrate by mechanically exfoliating bulk WSe_2 flakes using a poly(dimethylsiloxane) (PDMS) film. The layer numbers were confirmed based on the contrast of optical images on the SiO_2/n^+-Si substrate,[31] assisted by Raman spectroscopy. Following the resist pattering for source/drain electrodes performed via a maskless aligner, a low-concentration UV-ozone treatment of ∼5 ppm was applied for 5 min at RT to minimize resist residue in the contact area. Subsequently, Pt source/drain electrodes were deposited via either EB evaporation (AEV-HR1, AVC Corp.) or sputtering (QAM-4-ST, ULVAC Corp.). In the EB evaporation process, a 10 nm Pt film was initially deposited via EB evaporation, followed by a 20 nm Au film via thermal evaporation to increase the thickness of electrodes. During EB evaporation, on the other hand, the sample was maintained at RT through external cooling to reduce damage induced by radiation heating. The detailed device fabrication conditions are summarized in Figure S1. All electrical measurements were performed at RT by using a semiconductor parameter analyzer (Keysight, B1500A) in a vacuum prober.

Figure 1b shows the transfer characteristics of 1L-WSe_2 Schottky FETs with Pt electrodes, deposited via either EB evaporation or sputtering, as a function of the back gate voltage (V_{bg}). It should be noted that the device with sputtered Pt electrodes was annealed at 200 °C in an Ar/H_2 atmosphere for 10 min to reduce strain induced in Pt electrodes during the sputtering. This process proved to be effective in enhancing the transfer characteristics by stabilizing sputtered Pt electrodes, as shown in Figure S2. However, such an improvement was not observed in EB-evaporated Pt electrodes after annealing. It was anticipated that the 1L-WSe_2 FETs with Pt electrodes would exhibit p-type behavior due to the ideal band alignment with a negligible SBH for the valence band edge of WSe_2 and a large SBH exceeding 1 eV for the conduction band edge.[12,32] However, both WSe_2 FETs exhibited an ambipolar behavior. Additionally, a critical difference is the variation in the threshold voltage difference (ΔV_{th}) between the n- and p-branch in the FET operations, as shown in Figure 1b. This difference largely depends on the Pt deposition methods. The narrower ΔV_{th} in the FET with EB-evaporated electrodes implies a reduction in the effective SBHs for the conduction band edge of WSe_2, likely due to the formation of numerous defect states in WSe_2 during Pt deposition. Although the WSe_2 channel was maintained at RT through external cooling during EB evaporation to mitigate damages induced by radiation heating,[28] secondary or backscattered electrons might still contribute to the degradation of the WSe_2 channel. In contrast, the 1L-WSe_2 FET with sputtered Pt electrodes exhibited a wider ΔV_{th}, which could enhance the p-type operation of the WSe_2 FET by ensuring a stable off-state across a wider gate voltage range. The detail of the relationship between ΔV_{th} and the effective SBH is described in Figure S3. The wider ΔV_{th} implies that the defect states density at the metal/WSe_2 interface generated by sputtering is lower than that produced by EB evaporation, contrary to our intuition.

Based solely on these implications, the expected band alignments at the Pt/WSe_2 interfaces are schematically summarized in Figure 1c under the assumption that the defect states associated with EB-evaporated Pt electrodes are symmetrically distributed within the band gap of WSe_2. However, this interpretation appears to contradict the widely accepted understanding that sputtering processes induce more damage to the underlying material than EB evaporation.[17] Indeed, through subsequent investigations, we show that this initial assumption regarding the band alignment was fundamentally incorrect.

Next, the impact of Pt deposition on the structural and electronic properties of WSe_2 is examined using X-ray photoelectron spectroscopy (XPS), Raman spectroscopy, and

https://doi.org/10.1021/acsomega.5c05764
ACS Omega 2025, 10, 42973−42979

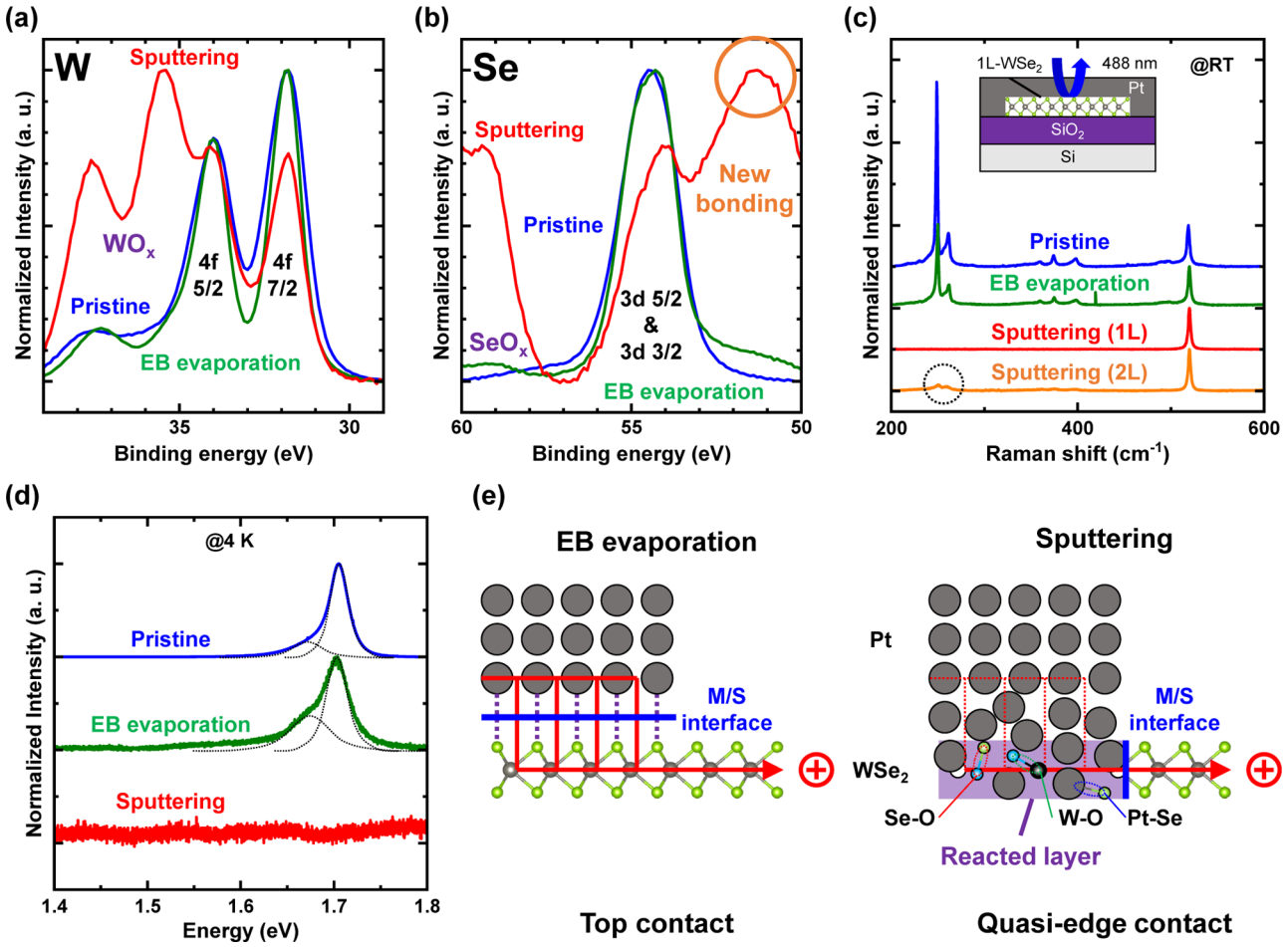

Figure 2. XPS spectra of (a) W and (b) Se obtained from CVD-grown 1L-WSe_2 measured before and after Pt deposition. (c) Raman spectra of exfoliated 1L-WSe_2 measured before and after Pt deposition. (d) PL spectra of 1L-WSe_2 measured before and after Pt deposition. (e) Schematic illustration of the expected Pt/WSe_2 interfaces for EB evaporation and sputtering.

photoluminescence (PL) spectroscopy to elucidate the differences in FET characteristics and deposition-induced damage associated with various deposition methods. For the XPS analysis, 1L-WSe_2 grown on a sapphire substrate via chemical vapor deposition (CVD) was employed instead of exfoliated flakes since a large surface area is required for XPS measurements. A 1 nm Pt film was deposited via either EB evaporation or sputtering onto the entire 1 × 1 cm^2 1L-WSe_2/sapphire substrate. The core-level spectra of W 4f and Se 3d are shown in Figure 2a and b, respectively. The sample with the EB-evaporated Pt film exhibited minimal changes in the core-level peaks of W and Se, while the sample with the sputtered Pt film exhibited new peaks at 37.6, 35.4, and 59.4 eV on the higher binding energy side of the initial peaks. These new peaks are likely attributable to the formation of WO_x and SeO_x,[33,34] and their emergence would be ascribed to residual oxygen within the sputtering chamber or exposure to air prior to the XPS measurement. This indicates that WSe_2 undergoes degradation during the Pt sputtering process. Furthermore, another peak appeared at around 51.3 eV on the lower binding energy side of the initial Se 3d peak, which likely suggests the formation of $PtSe_x$ compounds as a result of the Pt sputtering process, given the electronegativities of Pt (2.28) and Se (2.05).

Raman spectroscopy using a 488 nm semiconductor laser was performed at RT on 1L-WSe_2 exfoliated on a 90 nm SiO_2/n^+-Si substrate, both before and after Pt deposition. For a fair comparison, all spectra were normalized to the intensity of the Si substrate peak around 520 cm^{-1}, as shown in Figure 2c. The two main peaks of 1L-WSe_2, observed around 250 cm^{-1} and corresponding to E^1_{2g} and A_{1g} modes,[35] were clearly present even after EB evaporation of Pt, suggesting that the crystal structure of 1L-WSe_2 was preserved after EB evaporation of Pt. However, these peaks were absent in 1L-WSe_2 after Pt sputtering, indicating the disruption of the crystal structure of WSe_2. The significant diminution of these peaks even in 2L-WSe_2 after Pt sputtering exhibited adverse effects on the underlying layer of WSe_2, as well as on the top layer. Moreover, PL measurements were also performed at 4 K to investigate the electronic structure of 1L-WSe_2, as shown in Figure 2d. The samples used for PL measurements were identical to those used for Raman measurements. Each spectrum was normalized to the maximum peak intensity except for that of Pt-sputtered 1L-WSe_2. The PL peaks corresponding to the exciton (1.71 eV) and trion (1.68 eV)[36,37] were absent in 1L-WSe_2 after Pt sputtering, suggesting that the Pt sputtering process enhances nonradiative recombination or induces significant degradation in the band structure of 1L-WSe_2.

Although the 1L-WSe_2 device with sputtered Pt electrodes showed FET operation, XPS, Raman spectroscopy, and PL analyses indicated that the crystal integrity was not preserved. Here, let us consider the interface structure of EB-evaporated

https://doi.org/10.1021/acsomega.5c05764
ACS Omega 2025, 10, 42973−42979

and sputtered Pt/WSe_2 devices. In the case of EB evaporation, evaporated Pt is unlikely to chemically react with WSe_2, as evidenced by the minimal qualitative changes observed in XPS, Raman, and PL spectra. A Schottky junction is therefore expected to form at the Pt/WSe_2 interface as a conventional top contact in the out-of-plane direction, as schematically illustrated in Figure 2e. Despite the minimal reaction, the effective SB lowering expected from the narrower ΔV_{th} in Figure 1b suggests that defects are generated in 1L-WSe_2 under the EB-evaporated Pt electrode. In contrast, the Pt-sputtered 1L-WSe_2 did not preserve an ideal Pt/WSe_2 interface but instead will form a reacted layer comprising other compounds, such as oxides or selenides as identified through XPS analysis (additional characterization is shown in Figure S4). Nevertheless, the FET operation with a wider ΔV_{th} was observed. The high power of Pt sputtering could lead to different contact geometries as well as high-density defect formation. That is, this FET operation could be interpreted within a model where the Schottky junction is likely formed not between Pt and the reacted layer but rather between the reacted layer and WSe_2, functioning as a quasi-edge contact in the in-plane direction. In this model, almost no potential barrier would exist at the interface between sputtered Pt and the reacted layer, meaning the reacted layer would act as a metallic layer. 200 °C annealing after Pt sputtering would enhance the metallization of the reacted layer. The wider ΔV_{th} in Figure 1b suggests a relatively lower defect state density at the interface between the reacted layer and WSe_2. Small I_d values could also be explained by the small contact area of the quasi-edge contact. Compared with the conventional edge contact fabrication process,[38] the present study will provide alternative process for edge contact formation without channel etching and precise control of position alignment.

From several characterizations, a quasi-edge contact between sputtered Pt electrodes and WSe_2 was suggested. Since this current injection mechanism differs from that of the conventional top contact formed via EB evaporation, the performance and contact resistance of p-FETs after contact doping might be improved. Therefore, it would be worth exploring the feasibility of sputtered Pt contacts on WSe_2 by evaluating them.[39] Although molecular doping[40] is commonly employed in the research of 2D semiconductors, it is incompatible with the practical FET fabrication process that involves thermal annealing. In this work, charge transfer from WO_x formed by self-limiting layer-by layer oxidation was selected due to its stable and reliable doping mechanism.[41−43] Since the Fermi level in WO_3 is located below the conduction band composed of empty d states, WO_3 can possess a high work function of ∼6.5 eV.[44] Figure 3a illustrates the schematic of contact doping via ozone oxidation. The depletion layer of WSe_2 at the metal/WSe_2 contact becomes thinner due to hole doping from WO_x, resulting in a more efficient hole injection. Compared to our previous studies on p-WSe_2 operation using thermally evaporated Au electrodes and hole transfer from WO_x,[39] the use of sputtered Pt source/drain electrodes may also contribute to enhance hole injection by lowering the Fermi level. To surely maintain the continuous WSe_2 channel layer even after oxidation of the top WSe_2 layer, 2L-WSe_2 was selected. The details are described in Figure S5. For the fabrication of the 2L-WSe_2 FET, the WSe_2 channel transferred onto a SiO_2/n^+-Si substrate was first patterned by CF_4 plasma etching. Hexagonal boron nitride (h-BN) was then transferred as a top gate insulator using a PDMS film, with the thickness of

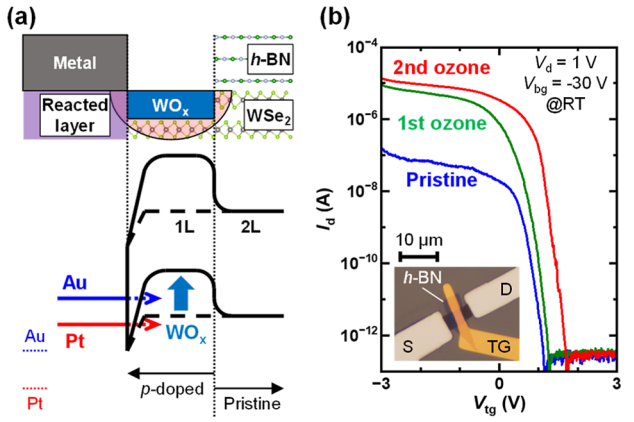

Figure 3. (a) Schematic illustration showing the cross-sectional device view in the vicinity of the contact area after ozone oxidation, along with the corresponding electronic band diagram of 2L-WSe_2 FET. (b) I_d−V_{tg} characteristics of the 2L-WSe_2 FET with sputtered Pt electrodes, measured before and after ozone oxidation at a constant V_d of 1 V at RT. The inset shows an optical image of the device after the second ozone oxidation.

the h-BN layer measured at 10.2 nm via atomic force microscopy (AFM) measurement. Subsequently, Pt source/drain electrodes were sputtered, and the Au top gate electrode was thermally evaporated. The device was subsequently annealed to stabilize the sputtered Pt electrodes. Finally, hole doping into WSe_2 was introduced by UV-ozone oxidation at a concentration of ∼650 ppm and 60 °C. Electrical measurements were performed before and after ozone oxidation. Notably, this concentration for layer-by-layer oxidation is much higher than the concentration of ∼5 ppm to minimize resist residue in the contact area.

Figure 3b shows the transfer characteristics of the 2L-WSe_2 FET before and after hole doping via ozone oxidation as a function of top gate voltage (V_{tg}). It is important to note that the operation mechanism of this top-gate WSe_2 FET adheres to the principles of the MOSFET. The inset of Figure 3b presents an optical image of the device after ozone oxidation. The on-current in p-FET operation increased from 10^{-7} A to 10^{-5} A after a 10 min ozone oxidation process. Furthermore, an additional 20 min of ozone oxidation further enhanced the on-current and induced a positive V_{th} shift, indicating further hole doping and a notable reduction in contact resistance with prolonged oxidation. However, the optical contrast on the uncovered area of the WSe_2 channel did not change even after the additional ozone oxidation, as shown in Figure S6a, suggesting that only a very small area of WSe_2 was converted to WO_x. This observation aligns with the previous TEM observation.[39] The subthreshold swing (SS), field-effect mobility (μ_{FE}), and contact resistance (R_c) were extracted from the transfer characteristics obtained after the additional ozone oxidation, as detailed in Figure S6b−e. The SS and μ_{FE} were estimated to be ∼110 mV dec^{-1} and ∼37 cm^2 V^{-1} s^{-1}, respectively. Since R_c can be assumed as a constant value independent of V_{tg} for the top gate structure, the Y-function method,[45−47] which is applicable to individual two-terminal devices with constant R_c, was employed to evaluate R_c. Using the Y function ($Y = I_d/\sqrt{g_m}$, where g_m is the transconductance), R_c was calculated to be ∼3.7 × 10^2 kΩ μm. This value, while higher than initially anticipated, is notably comparable to those obtained in our previous studies on the h-BN top-gate WSe_2 FET with Au source/drain electrodes and

https://doi.org/10.1021/acsomega.5c05764
ACS Omega 2025, 10, 42973−42979

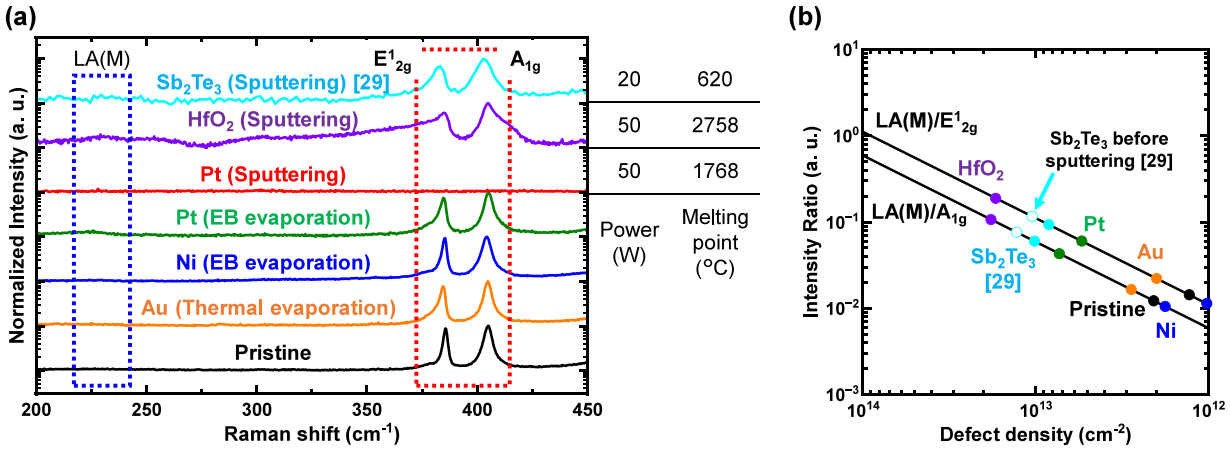

Figure 4. (a) Raman spectra of 1L-MoS_2 measured before and after the deposition of various materials. The spectrum for SB_2Te_3-sputtered MoS_2 is cited from ref 29. The applied sputtering power and melting points of Pt, HfO_2, and Sb_2Te_3 are denoted alongside. (b) Defect densities in 1L-MoS_2 estimated from the relative intensity of the LA(M) peak to the A_{1g} peak. (a) Adapted from W. H. Chang et al., Adv. Electron. Mater. 2023, 9, 2201091. Published under a Creative Commons Attribution License (CC BY 4.0).

hole transfer from WO_x.[39] Figure S7 compares the transfer characteristics, optical images, and the extracted values of both devices. The comparable R_c values for Pt and Au electrodes strongly suggest that the p-FET performance of WSe_2 FETs with ozone oxidation is primarily governed by charge transfer from WO_x rather than the SBH at the metal/WSe_2 interface.

Interfacial density states density (D_{it}) distribution within the band gap of WSe_2, particularly near the valence band, can be extracted from the curve fitting of the transfer characteristics. The detailed method and the result of D_{it} extraction are described in Figure S8.

In contrast, vdW contacts such as Sb_2Te_3/MoS_2 and Bi_2Te_3/WSe_2 have been successfully achieved through sputtering methods.[29,30] Therefore, the relation between deposition techniques, deposited materials, and defect density generated in 2D materials is further explored. For a more generalized discussion, mechanically exfoliated 1L-MoS_2 on a 90 nm SiO_2/n^+-Si substrate was utilized as a model 2D material, where the defect density has been quantitatively correlated with the intensity of Raman LA(M) around 230 cm^{-1}.[48] Figure 4a presents the Raman spectra of 1L-MoS_2 measured after the deposition of various materials with a few nanometer thickness.[29] All spectra are normalized to the intensity of the A_{1g} peak except for that of the sputtered Pt sample. Regarding the full width at half-maximum (fwhm) of the A_{1g} peak, no significant differences were observed between the pristine, thermally evaporated Au, EB-evaporated Ni, and EB-evaporated Pt samples. However, the fwhms in the sputtered Sb_2Te_3 and HfO_2 samples exhibited noticeable increases, and the peak disappeared in the Pt-sputtered sample, exhibiting behavior similar to that observed in WSe_2. To quantitatively evaluate the defect density in 1L-MoS_2,[48] the relative intensity of the LA(M) peak to the A_{1g} peak was analyzed, as shown in Figure 4b. Although the excitation wavelength (532 nm) in the original study differs from that used in this study (488 nm), it is assumed that this difference does not greatly affect the results. It should be noted that in the case of Sb_2Te_3 sputtering, MoS_2 already contained defect states of $\sim 1 \times 10^{13}$ cm^{-2} before sputtering because it was grown by CVD, with no significant increase in defect density after the sputtering process. In contrast, the defect density for HfO_2 sputtering was found to be $\sim 2 \times 10^{13}$ cm^{-2}, nearly double that for Sb_2Te_3 sputtering. This discrepancy could be caused by a difference in sputtering power. Conversely, despite the same power being used for both HfO_2 and Pt sputtering, the degree of crystal structure degradation was significantly different. This variation may be ascribed to the differing chemical reactivities of the materials involved. The Gibbs free energies of formation at 300 K for various compounds are summarized in Figure S9.[49] No spontaneous reaction is expected between MoS_2 (or WSe_2) and the materials (Pt, Au, HfO_2, and so on) employed in this research. However, when Pt is deposited on MoS_2 in the presence of O_2, the reaction $MoS_2 + 1/2\ Pt + 2O_2\ (g) \rightarrow MoO_2 + SO_2\ (g) + 1/2\ PtS_2$ is expected to occur spontaneously due to the negative Gibbs free energy change. A similar spontaneous reaction is also expected for WSe_2. Given the detection of WO_x and SeO_x by XPS, as shown in Figure 2a,b, this reaction likely occurred, driven by the high energy gain during sputtering. This emphasizes that residual oxygen during the sputtering of metal electrodes onto TMDCs must be carefully controlled.

CONCLUSION

In this study, p-FET performance was demonstrated even in the 1L-WSe_2 FET with sputtered Pt electrodes. Various characterization techniques, including XPS, PL, and Raman spectroscopy, elucidated that the crystal structure of WSe_2 was no longer preserved, suggesting the formation of a quasi-edge contact at the Pt/WSe_2 channel. From the perspective of sputtering applicability, the selection of deposited materials, the sputtering powers required for their deposition, and the control of residual O_2 are critical factors that must be carefully considered.

ASSOCIATED CONTENT

Supporting Information

The Supporting Information is available free of charge at https://pubs.acs.org/doi/10.1021/acsomega.5c05764.

The deposition condition of Pt, the effect of annealing after Pt deposition, the relationship between ΔV_{th} and effective SBH, the structural analysis of the reacted layer under sputtered Pt, the reason for 2L-WSe_2 selection for contact doping by layer-by layer oxidation, analysis of WSe_2 p-FET with sputtered Pt contact after additional

https://doi.org/10.1021/acsomega.5c05764
ACS Omega 2025, 10, 42973−42979

ozone oxidation, comparison to our previous research using evaporated Au contact, D_{it} extraction from curve fitting, and thermodynamics calculation between TMDCs and deposited materials (PDF)

AUTHOR INFORMATION

Corresponding Author

Kosuke Nagashio − *Department of Materials Engineering, The University of Tokyo, Tokyo 113-8656, Japan;* orcid.org/0000-0003-1181-8644; Email: nagashio@material.t.u-tokyo.ac.jp

Authors

Ryuichi Nakajima − *Department of Materials Engineering, The University of Tokyo, Tokyo 113-8656, Japan*

Tomonori Nishimura − *Department of Materials Engineering, The University of Tokyo, Tokyo 113-8656, Japan;* orcid.org/0000-0002-8000-5164

Kaito Kanahashi − *Department of Materials Engineering, The University of Tokyo, Tokyo 113-8656, Japan;* orcid.org/0000-0003-2571-3384

Shogo Hatayama − *Semiconductor Frontier Research Center, National Institute of Advanced Industrial Science and Technology (AIST), Ibaraki 305-8569, Japan;* orcid.org/0000-0002-2914-1072

Wen Hsin Chang − *Semiconductor Frontier Research Center, National Institute of Advanced Industrial Science and Technology (AIST), Ibaraki 305-8569, Japan;* orcid.org/0000-0002-8501-6276

Yuta Saito − *Device Technology Research Institute, National Institute of Advanced Industrial Science and Technology (AIST), Ibaraki 305-8569, Japan; Research Center for Green X-tech and Department of Materials Science, Tohoku University, Sendai, Miyagi 980-8579, Japan;* orcid.org/0000-0002-9576-1560

Toshifumi Irisawa − *Device Technology Research Institute, National Institute of Advanced Industrial Science and Technology (AIST), Ibaraki 305-8569, Japan*

Keiji Ueno − *Department of Chemistry, Saitama University, Saitama 338-8570, Japan*

Yasumitsu Miyata − *Department of Physics, Tokyo Metropolitan University, Tokyo 192-0397, Japan; Research Center for Materials Nanoarchitectonics, National Institute for Materials Science, Ibaraki 305-0044, Japan;* orcid.org/0000-0002-9733-5119

Takashi Taniguchi − *Research Center for Materials Nanoarchitectonics, National Institute for Materials Science, Ibaraki 305-0044, Japan;* orcid.org/0000-0002-1467-3105

Kenji Watanabe − *Research Center for Electronic and Optical Materials, National Institute for Materials Science, Ibaraki 305-0044, Japan;* orcid.org/0000-0003-3701-8119

Complete contact information is available at: https://pubs.acs.org/10.1021/acsomega.5c05764

Notes

The authors declare no competing financial interest.

ACKNOWLEDGMENTS

This research was supported by the JSPS KAKENHI (Grant Numbers: JP21H05237, JP21H05236, JP21H05232, JP21H05233, JP21K04826, JP22H04957, JP22K04212, JP22H05445, JP23K23243, JP23K02052, JP23K26745, and JP24K08195), the NICT (Grant Number: 05901), the JST-Mirai Program (Grant Number: JPMJMI22708192), the JST CREST (Grant Number: JPMJCR23A4, JPMJCR24A3, and JPMJCR24A5), the JST FOREST Program (Grant Number JPMJFR213X), and the World Premier International Research Center Initiative (WPI), MEXT, Japan.

REFERENCES

(1) Ago, H.; Okada, S.; Miyata, Y.; Matsuda, K.; Koshino, M.; Ueno, K.; Nagashio, K. Science of 2.5 Dimensional Materials: Paradigm Shift of Materials Science toward Future Social Innovation. *Sci. Technol. Adv. Mater.* **2022**, *23* (1), 275−299.

(2) Akinwande, D.; Huyghebaert, C.; Wang, C.-H.; Serna, M. I.; Goossens, S.; Li, L.-J.; Wong, H.-S. P.; Koppens, F. H. L. Graphene and Two-Dimensional Materials for Silicon Technology. *Nature* **2019**, *573* (7775), 507−518.

(3) Desai, S. B.; Madhvapathy, S. R.; Sachid, A. B.; Llinas, J. P.; Wang, Q.; Ahn, G. H.; Pitner, G.; Kim, M. J.; Bokor, J.; Hu, C.; Wong, H.-S. P.; Javey, A. MoS_2 Transistors with 1-Nanometer Gate Lengths. *Science* **2016**, *354* (6308), 99−102.

(4) Uchiyama, H.; Maruyama, K.; Chen, E.; Nishimura, T.; Nagashio, K. A Monolayer MoS_2 FET with an EOT of 1.1 Nm Achieved by the Direct Formation of a High-κ Er_2O_3 Insulator Through Thermal Evaporation. *Small* **2023**, *19* (15), 2207394.

(5) Li, W.; Zhou, J.; Cai, S.; Yu, Z.; Zhang, J.; Fang, N.; Li, T.; Wu, Y.; Chen, T.; Xie, X.; Ma, H.; Yan, K.; Dai, N.; Wu, X.; Zhao, H.; Wang, Z.; He, D.; Pan, L.; Shi, Y.; Wang, P.; Chen, W.; Nagashio, K.; Duan, X.; Wang, X. Uniform and Ultrathin High-κ Gate Dielectrics for Two-Dimensional Electronic Devices. *Nat. Electron.* **2019**, *2* (12), 563−571.

(6) Houssa, M.; Dimoulas, A.; Molle, A.. In *2D Materials for Nanoelectronics*; Houssa, M., Dimoulas, A., Molle, A., Eds.; CRC Press, 2016.

(7) Fang, N.; Nagashio, K. Accumulation-Mode Two-Dimensional Field-Effect Transistor: Operation Mechanism and Thickness Scaling Rule. *ACS Appl. Mater. Interfaces* **2018**, *10* (38), 32355−32364.

(8) Das, S.; Chen, H.-Y.; Penumatcha, A. V.; Appenzeller, J. High Performance Multilayer MoS_2 Transistors with Scandium Contacts. *Nano Lett.* **2013**, *13* (1), 100−105.

(9) Kim, C.; Moon, I.; Lee, D.; Choi, M. S.; Ahmed, F.; Nam, S.; Cho, Y.; Shin, H.-J.; Park, S.; Yoo, W. J. Fermi Level Pinning at Electrical Metal Contacts of Monolayer Molybdenum Dichalcogenides. *ACS Nano* **2017**, *11* (2), 1588−1596.

(10) Liu, Y.; Guo, J.; Zhu, E.; Liao, L.; Lee, S.-J.; Ding, M.; Shakir, I.; Gambin, V.; Huang, Y.; Duan, X. Approaching the Schottky−Mott Limit in van Der Waals Metal−Semiconductor Junctions. *Nature* **2018**, *557* (7707), 696−700.

(11) Sotthewes, K.; van Bremen, R.; Dollekamp, E.; Boulogne, T.; Nowakowski, K.; Kas, D.; Zandvliet, H. J. W.; Bampoulis, P. Universal Fermi-Level Pinning in Transition-Metal Dichalcogenides. *J. Phys. Chem. C* **2019**, *123* (9), 5411−5420.

(12) Michaelson, H. B. The Work Function of the Elements and Its Periodicity. *J. Appl. Phys.* **1977**, *48* (11), 4729−4733.

(13) Ni, Z. H.; Wang, H. M.; Ma, Y.; Kasim, J.; Wu, Y. H.; Shen, Z. X. Tunable Stress and Controlled Thickness Modification in Graphene by Annealing. *ACS Nano* **2008**, *2* (5), 1033−1039.

(14) Qiu, X. P.; Shin, Y. J.; Niu, J.; Kulothungasagaran, N.; Kalon, G.; Qiu, C.; Yu, T.; Yang, H. Disorder-Free Sputtering Method on Graphene. *AIP Adv.* **2012**, *2* (3), 032121.

(15) Shi, W.; Lin, M.-L.; Tan, Q.-H.; Qiao, X.-F.; Zhang, J.; Tan, P.-H. Raman and Photoluminescence Spectra of Two-Dimensional Nanocrystallites of Monolayer WS_2 and WSe_2. *2d Mater.* **2016**, *3* (2), 025016.

(16) Wu, Z.; Zhao, W.; Jiang, J.; Zheng, T.; You, Y.; Lu, J.; Ni, Z. Defect Activated Photoluminescence in WSe_2 Monolayer. *J. Phys. Chem. C* **2017**, *121* (22), 12294−12299.

(17) Telkhozhayeva, M.; Girshevitz, O. Roadmap toward Controlled Ion Beam-Induced Defects in 2D Materials. *Adv. Funct. Mater.* **2024**, *34* (45), 2404615.
(18) Tosun, M.; Chuang, S.; Fang, H.; Sachid, A. B.; Hettick, M.; Lin, Y.; Zeng, Y.; Javey, A. High-Gain Inverters Based on WSe_2 Complementary Field-Effect Transistors. *ACS Nano* **2014**, *8* (5), 4948−4953.
(19) Lee, I.; Rathi, S.; Li, L.; Lim, D.; Atif Khan, M.; Kannan, E. S.; Kim, G.-H. Non-Degenerate n-Type Doping by Hydrazine Treatment in Metal Work Function Engineered WSe_2 Field-Effect Transistor. *Nanotechnology* **2015**, *26* (45), 455203.
(20) Yu, L.; Zubair, A.; Santos, E. J. G.; Zhang, X.; Lin, Y.; Zhang, Y.; Palacios, T. High-Performance WSe_2 Complementary Metal Oxide Semiconductor Technology and Integrated Circuits. *Nano Lett.* **2015**, *15* (8), 4928−4934.
(21) Jo, S.; Kang, D.; Shim, J.; Jeon, J.; Jeon, M. H.; Yoo, G.; Kim, J.; Lee, J.; Yeom, G. Y.; Lee, S.; Yu, H.; Choi, C.; Park, J. A High-Performance WSe_2/*h*-BN Photodetector Using a Triphenylphosphine (PPh_3)-Based N-Doping Technique. *Adv. Mater.* **2016**, *28* (24), 4824−4831.
(22) Ma, Z.; Zhang, L.; Zhou, C.; Chan, M. High Current Nb-Doped P-Channel MoS_2 Field-Effect Transistor Using Pt Contact. *IEEE Electron Device Lett.* **2021**, *42* (3), 343−346.
(23) Li, S.; Wu, Q.; Ding, H.; Wu, S.; Cai, X.; Wang, R.; Xiong, J.; Lin, G.; Huang, W.; Chen, S.; Li, C. High Gain, Broadband p-WSe_2/n-Ge van Der Waals Heterojunction Phototransistor with a Schottky Barrier Collector. *Nano Res.* **2023**, *16* (4), 5796−5802.
(24) Patoary, N. H.; Xie, J.; Zhou, G.; Al Mamun, F.; Sayyad, M.; Tongay, S.; Esqueda, I. S. Improvements in 2D P-Type WSe_2 Transistors towards Ultimate CMOS Scaling. *Sci. Rep.* **2023**, *13* (1), 3304.
(25) Takeyama, K.; Moriya, R.; Watanabe, K.; Masubuchi, S.; Taniguchi, T.; Machida, T. Low-Temperature p-Type Ohmic Contact to WSe_2 Using p^+-MoS_2/WSe_2 van Der Waals Interface. *Appl. Phys. Lett.* **2020**, *117* (15), 153101.
(26) Movva, H. C. P.; Rai, A.; Kang, S.; Kim, K.; Fallahazad, B.; Taniguchi, T.; Watanabe, K.; Tutuc, E.; Banerjee, S. K. High-Mobility Holes in Dual-Gated WSe_2 Field-Effect Transistors. *ACS Nano* **2015**, *9* (10), 10402−10410.
(27) Nazir, G.; Kim, H.; Kim, J.; Kim, K. S.; Shin, D. H.; Khan, M. F.; Lee, D. S.; Hwang, J. Y.; Hwang, C.; Suh, J.; Eom, J.; Jung, S. Ultimate Limit in Size and Performance of WSe_2 Vertical Diodes. *Nat. Commun.* **2018**, *9* (1), 5371.
(28) Wang, Y.; Kim, J. C.; Li, Y.; Ma, K. Y.; Hong, S.; Kim, M.; Shin, H. S.; Jeong, H. Y.; Chhowalla, M. P-Type Electrical Contacts for 2D Transition-Metal Dichalcogenides. *Nature* **2022**, *610* (7930), 61−66.
(29) Chang, W. H.; Hatayama, S.; Saito, Y.; Okada, N.; Endo, T.; Miyata, Y.; Irisawa, T. Sb_2Te_3/MoS_2 Van Der Waals Junctions with High Thermal Stability and Low Contact Resistance. *Adv. Electron Mater.* **2023**, *9* (4), 2201091.
(30) Chang, W. H.; Hatayama, S.; Saito, Y.; Okada, N.; Endo, T.; Miyata, Y.; Irisawa, T. Thermally Stable Bi_2Te_3/WSe_2 Van Der Waals Contacts for PMOSFETs Application. *Sci. Rep.* **2024**, *14* (1), 28572.
(31) Hsu, C.; Frisenda, R.; Schmidt, R.; Arora, A.; de Vasconcellos, S. M.; Bratschitsch, R.; van der Zant, H. S. J.; Castellanos-Gomez, A. Thickness-Dependent Refractive Index of 1L, 2L, and 3L MoS_2, $MoSe_2$, WS_2, and WSe_2. *Adv. Opt. Mater.* **2019**, *7* (13), 1900239.
(32) Guo, Y.; Robertson, J. Band Engineering in Transition Metal Dichalcogenides: Stacked versus Lateral Heterostructures. *Appl. Phys. Lett.* **2016**, *108* (23), 233104.
(33) Jaegermann, W.; Schmeisser, D. Reactivity of Layer Type Transition Metal Chalcogenides towards Oxidation. *Surf. Sci.* **1986**, *165* (1), 143−160.
(34) Smyth, C. M.; Addou, R.; McDonnell, S.; Hinkle, C. L.; Wallace, R. M. WSe_2-Contact Metal Interface Chemistry and Band Alignment under High Vacuum and Ultra High Vacuum Deposition Conditions. *2d Mater.* **2017**, *4* (2), 025084.
(35) Luo, X.; Zhao, Y.; Zhang, J.; Toh, M.; Kloc, C.; Xiong, Q.; Quek, S. Y. Effects of Lower Symmetry and Dimensionality on Raman Spectra in Two-Dimensional WSe_2. *Phys. Rev. B* **2013**, *88* (19), 195313.
(36) Wang, G.; Bouet, L.; Lagarde, D.; Vidal, M.; Balocchi, A.; Amand, T.; Marie, X.; Urbaszek, B. Valley Dynamics Probed through Charged and Neutral Exciton Emission in Monolayer WSe_2. *Phys. Rev. B* **2014**, *90* (7), 075413.
(37) Jones, A. M.; Yu, H.; Ross, J. S.; Klement, P.; Ghimire, N. J.; Yan, J.; Mandrus, D. G.; Yao, W.; Xu, X. Spin-Layer Locking Effects in Optical Orientation of Exciton Spin in Bilayer WSe_2. *Nat. Phys.* **2014**, *10* (2), 130−134.
(38) Ngo, T. D.; Choi, M. S.; Lee, M.; Ali, F.; Yoo, W. J. Anomalously Persistent P-Type Behavior of WSe_2 Field-Effect Transistors by Oxidized Edge-Induced Fermi-Level Pinning. *J. Mater. Chem. C Mater.* **2022**, *10* (3), 846−853.
(39) Kato, R.; Uchiyama, H.; Nishimura, T.; Ueno, K.; Taniguchi, T.; Watanabe, K.; Chen, E.; Nagashio, K. P-Type Conversion of WS_2 and WSe_2 by Position-Selective Oxidation Doping and Its Application in Top Gate Transistors. *ACS Appl. Mater. Interfaces* **2023**, *15* (22), 26977−26984.
(40) Ji, H. G.; Solís-Fernández, P.; Yoshimura, D.; Maruyama, M.; Endo, T.; Miyata, Y.; Okada, S.; Ago, H. Chemically Tuned P-and N-Type WSe_2 Monolayers with High Carrier Mobility for Advanced Electronics. *Adv. Mater.* **2019**, *31* (42), 1903613.
(41) Yamamoto, M.; Dutta, S.; Aikawa, S.; Nakaharai, S.; Wakabayashi, K.; Fuhrer, M. S.; Ueno, K.; Tsukagoshi, K. Self-Limiting Layer-by-Layer Oxidation of Atomically Thin WSe_2. *Nano Lett.* **2015**, *15* (3), 2067−2073.
(42) Yamamoto, M.; Nakaharai, S.; Ueno, K.; Tsukagoshi, K. Self-Limiting Oxides on WSe_2 as Controlled Surface Acceptors and Low-Resistance Hole Contacts. *Nano Lett.* **2016**, *16* (4), 2720−2727.
(43) He, J.; Fang, N.; Nakamura, K.; Ueno, K.; Taniguchi, T.; Watanabe, K.; Nagashio, K. 2D Tunnel Field Effect Transistors (FETs) with a Stable Charge-Transfer-Type p^+-WSe_2 Source. *Adv. Electron Mater.* **2018**, *4* (7), 1800207.
(44) Greiner, M. T.; Lu, Z.-H. Thin-Film Metal Oxides in Organic Semiconductor Devices: Their Electronic Structures, Work Functions and Interfaces. *NPG Asia Mater.* **2013**, *5* (7), No. e55.
(45) Ghibaudo, G. New Method for the Extraction of MOSFET Parameters. *Electron. Lett.* **1988**, *24* (9), 543−545.
(46) Chang, H.-Y.; Zhu, W.; Akinwande, D. On the Mobility and Contact Resistance Evaluation for Transistors Based on MoS_2 or Two-Dimensional Semiconducting Atomic Crystals. *Appl. Phys. Lett.* **2014**, *104* (11), 113504.
(47) Liu, C.; Xu, Y.; Noh, Y.-Y. Contact Engineering in Organic Field-Effect Transistors. *Mater. Today* **2015**, *18* (2), 79−96.
(48) Mignuzzi, S.; Pollard, A. J.; Bonini, N.; Brennan, B.; Gilmore, I. S.; Pimenta, M. A.; Richards, D.; Roy, D. Effect of Disorder on Raman Scattering of Single-Layer MoS_2. *Phys. Rev. B* **2015**, *91* (19), 195411.
(49) Chang, Y.-R.; Nishimura, T.; Nagashio, K. Thermodynamic Perspective on the Oxidation of Layered Materials and Surface Oxide Amelioration in 2D Devices. *ACS Appl. Mater. Interfaces* **2021**, *13* (36), 43282−43289.

https://doi.org/10.1021/acsomega.5c05764
ACS Omega 2025, 10, 42973−42979